Numerical studies of localized wavefields governed by the Raman-extended derivative nonlinear Schrödinger equation

1997 J. Phys. A: Math. Gen. 30 8207

(http://iopscience.iop.org/0305-4470/30/23/019)

J. Phys. A: Math. Gen. **30** (1997) 8207–8224. Printed in the UK PII: S0305-4470(97)85053-6

Numerical studies of localized wavefields governed by the Raman-extended derivative nonlinear Schrödinger equation

J S Hesthaven†, J Juul Rasmussen‡¶, L Bergé§ and J Wyller‖+

† Division of Applied Mathematics, Brown University, Box F, Providence, RI 02912, USA

‡ Optics and Fluid Dynamics Department, Risø National Laboratory, PO Box 49, 4000 Roskilde, Denmark

§ Commissariat à l'Energie Atomique, Centre d'Etudes de Limeil-Valenton, 94195 Villeneuve-Saint-Georges cedex, France

‖ Department of Mathematics, Narvik Institute of Technology, PO Box 385, N-8501 Narvik, Norway

Received 16 June 1997

Abstract. Using a stable pseudospectral multi-domain method we investigate the dynamics of localized wavefields in the extended derivative nonlinear Schrödinger equation, with particular emphasis on the critical mass and structure of the initial conditions that promote wave collapse. The results are found to correspond well with theoretical observations based on a Lagrangian approach and through comparison with solutions of the critical nonlinear Schrödinger equation. Inclusion of high-order nonlinear dissipation due to the self-induced Raman effect, leading to the Raman-extended derivative nonlinear Schrödinger equation, is found to inhibit finite-time collapse in certain cases.

1. Introduction

In the quasi-monochromatic approximation, high-frequency waves evolving in nonlinear dispersive media are usually analysed in the framework of the nonlinear Schrödinger (NLS) equation, which formally follows from a straightforward Taylor expansion of the nonlinear dispersion law $\omega = \omega(k, |E|^2)$, around the point $\omega_0 = \omega(k_0, 0)$ attached to the unperturbed wave with frequency ω_0, wave number k_0 and amplitude E. This equation is widely applied in many branches of physics, as in nonlinear optics [1]. Here, recent progress in theory and experiments on soliton transmission systems with ultrashort pulses has raised an increasing interest in view of realizing ultrahigh-speed communications. For ultrashort pulses with a temporal width of the order of a few picoseconds, the width of the frequency spectrum, $\Delta\omega$, related to the inverse pulsewidth $(2t_0)^{-1}$, is rather large and allows for the occurrence of high-order dispersive effects, such as nonlinear dispersion and the so-called self-induced Raman effect [2].

More precisely, for an optical pulse propagating through a monomode dielectric guide with a nonlinear refraction index, Maxwell equations, governing the electric field E, can be expanded with respect to the scaling parameter $\epsilon = \mathrm{O}(\Delta\omega/\omega_0)$, which remains small in

¶ Corresponding author

+ Present Address: Department of Mathematical Sciences, The Agricultural University of Norway, PO Box 5035, N-1432 Ås, Norway.

0305-4470/97/238207+18$19.50

the quasi-monochromatic approximation. In this approximation, the resulting propagation equation applies to the evolution of extended wavepackets whose temporal and spatial spectra are narrow enough, i.e. $\Delta\omega/\omega_0 \sim \Delta k/k_0 \sim \epsilon \ll 1$, for a Kerr-type material with a linear refraction index n_0 and a small change in the dielectric constant $\Delta n/n_0 \sim \epsilon^2$. This modification of the refraction index follows from the dependence of the medium on the wavefield intensity, and the dispersion relation takes the perturbed form: $\omega = \omega(k, |E|^2)$. By making use of the slowly varying envelope substitution

$$E(x, t) = \mathrm{Re}\{\psi(x, t)\exp(\mathrm{i}\omega_0 t - \mathrm{i}k_0 x)\}$$

the electric-field envelope of the beam, ψ, is found to obey the well known NLS equation

$$2\mathrm{i}\partial_t\psi - \omega''\partial_\xi^2\psi + 2\alpha|\psi|^2\psi = 0 \tag{1}$$

to leading order. Here the variable $\xi = x - V_g^L t$ is a retarded space variable depending on the group velocity of linear waves $V_g^L = (\partial\omega/\partial k)|_{k=k_0}$, $\omega'' = (\partial^2\omega/\partial k^2)|_{k=k_0}$ denotes the usual dispersion coefficient and $\alpha = (\partial\omega/\partial|\psi|^2)|_{k=k_0}$ is a parameter related to the nonlinear frequency shift. An alternative formulation of equation (1), in which the space variable ξ is replaced by a retarded time variable and the temporal coordinate t by the propagation distance x, can also be derived when the dispersion relation of the waves is expressed in terms of $k(\omega, |\psi|^2)$ [2].

For wavepackets several wavelengths long with $\Delta\lambda/\lambda_0 > 1$ and for ultrashort wavetrains, the spectrum may not be narrow, which hence requires to take higher-order terms into account and to partly discard the previous approximation. As waves of different k can have different phase and group velocities, the latter may be sensitive in turn to the local wave intensity. Thus, an implicit dependence may exist between ω, k and $|\psi|^2$, yielding non-trivial second-order terms with dispersion coefficients such as, for example $\partial^2\omega/\partial k\partial|\psi|^2$, in the previous expansion of $\omega(k, |\psi|^2)$ around ω_0 and k_0. Among those extra terms, nonlinear dispersion arises in equation (1) as a nonlinear derivative: $\mathrm{i}|\psi|^2\partial_\xi\psi$ and nonlinear dissipation due to the self-induced Raman effect occurs in equation (1) in the form: $\psi\partial_\xi|\psi|^2$ [2, 3]. Moreover, considering intense wavetrains, one has to include quintic nonlinear effects proceeding from the power expansion of the dielectric constant in a series of the wavefield intensity, so that Kerr contributions in the form $|\psi|^4\psi$ must be retained in equation (1). Assuming $\omega'' < 0$, the final equation, expressed within the frame comoving with the linear group velocity V_g^L, results in the generalized NLS equation [4].

$$\mathrm{i}\partial_t\psi + \partial_\xi^2\psi = q_1|\psi|^2\psi + q_2|\psi|^4\psi + (q_3 + \mathrm{i}q_4)\psi\partial_\xi|\psi|^2 + \mathrm{i}q_5|\psi|^2\partial_\xi\psi \tag{2}$$

where $q_1, \ldots, q_5$ are real constants. Let us here recall that, strictly speaking, equation (2) should also contain higher-order dispersive terms involving the third-order derivative of the envelope ψ with respect to ξ. This derivative naturally emerges from the ordering $O(\epsilon^3)$ of the scale expansion of the combined Maxwell equations for the beam electric field in dielectric monomodes [2]. Furthermore, when considering high-order contributions such as quintic nonlinearities, it would seem natural to keep this third-order derivative as a significant dispersive term arising like $(\partial^3\omega/\partial k^3)\partial_\xi^3\psi$ from the Taylor expansion of the dispersion relation $\omega(k, |\psi|^2)$. Such a dispersive term may strongly modify the propagation of the envelope ψ, as shown in [2]. However, taking into account high-order nonlinear terms like those in equation (2) depends on the nonlinear response of the medium, whereas retaining the third-order derivative of the envelope is only justified from the dispersion properties of the medium. In what follows, we will consider a medium in which the nonlinear response is sufficiently strong to dominate over high-order dispersion, which means that the derivative $\partial_\xi^3\psi$ is assumed to be negligible, as compared with all the nonlinear

contributions in equation (2). This amounts to truncating the Taylor expansion of the above dispersion relation at the second order in k and $|\psi|^2$, as justified by considering a relatively flat dispersion profile.

From a mathematical point of view, equations in the form of equation (2) generally account for deviations from the standard ϵ-expansion corresponding to the so-called *marginal stable* case, for which the nonlinearity acts against the dispersion to a small extent only (see e.g. [5]). Also equation (2) is a model that exhibits wave collapse in the sense recalled below, and it is worthwhile only investigating the effects of nonlinear dispersion and dissipation on the collapse mechanism [4].

Equation (2) can be reduced to the convenient form ($\xi \to x$, $\psi \to u$)

$$\partial_t u + \mathrm{i}\partial_x^2 u + \beta|u|^2\partial_x u + \mathrm{i}\gamma u\partial_x|u|^2 + \mathrm{i}\sigma|u|^4 u = 0 \tag{3}$$

after using simple rescalings together with point and gauge transformations that the interested reader will find detailed in [4, 5]. Here, β refers to the coefficient of the nonlinear dispersion, γ is related to the Raman effect and σ, henceforth chosen to be positive for describing self-focusing regimes, is the nonlinearity coefficient attached to the Kerr effect.

In the absence of the two nonlinear derivatives ($\beta = \gamma = 0$), equation (3) simplifies to the critical nonlinear Schrödinger (CNLS) equation

$$-\mathrm{i}\partial_t u + \partial_x^2 u + \sigma|u|^4 u = 0 \tag{4}$$

which admits, for $\sigma > 0$, solutions that collapse in finite time, provided the energy integral $H_{\mathrm{CNLS}} = \int (|u_x|^2 - (\sigma/3)|u|^6)\,\mathrm{d}x$ is negative. This sufficient condition for collapse implies that the initial data $u(x, 0)$ possess a mass integral $N = \int |u|^2\,\mathrm{d}x$ above a critical threshold N_0. For $\sigma = 1$, this quantity, N_0, takes the value $N_0 \simeq 2.72$, as it results from the mass integral computed on the soliton solution $u(x, t) = \phi(x)\exp(-\mathrm{i}\lambda t)$ of equation (4) with $\lambda > 0$ and $|\phi(x)|^2 = \sqrt{3\lambda}/\cosh(2\sqrt{\lambda}x)$.

To analyse the effect of nonlinear dispersion ($\beta \neq 0$) on wave propagation, we can totally ignore the Kerr contribution together with the Raman delaying effect by setting $\sigma = \gamma = 0$ and in addition omit the linear dispersion term $\partial_x^2 u$ in equation (3). By doing so, we observe that the mass density of the wavefield obeys the continuity equation

$$\partial_t|u|^2 + \frac{\beta}{2}\partial_x(|u|^2 \cdot |u|^2) = 0 \tag{5}$$

which emphasizes that the wavepacket is being displaced along the x axis with a group velocity containing a nonlinear contribution proportional to the wave intensity: $\mathrm{d}x/\mathrm{d}t = \Delta V_{\mathrm{g}}^{\mathrm{NL}} = (\beta/2)|u|^2$. As a result, the sections of the wavepacket with different intensities move along x with different group velocities. For $\beta > 0$, the sections of the wavefield with higher intensities have higher velocities, which leads to an increase in the steepness of the leading edge of an initially symmetric wavepacket. For $\beta < 0$, nonlinear dispersion consistently causes opposite effects on the wavefield propagation. In what follows, we will always consider the case of a positive β for the sake of simplicity and set $\beta = 1$ for technical convenience.

Concerning the complete equation (3), it was speculated in [4] that for $\sigma > 0$ and $\gamma = 0$, i.e. without the Raman term, localized wavepackets with a sufficiently large mass ($N > 3\sigma N_0/\sqrt{12\sigma^2 + 9\sigma}$) should collapse in finite time, while waves with lower masses should remain regular, even asymptotically disperse, in a way similar to the spreading/blowing up of CNLS solutions. In the presence of the self-induced Raman effect ($\gamma \neq 0$), it was, moreover, expected on the basis of a variational (Lagrangian) approach that collapse might be arrested under certain conditions.

This paper is devoted to clarifying the previous theoretical speculations by means of accurate numerical simulations. In section 2, we recall some elements of related theory to equation (3), hereafter called the Raman-extended derivative nonlinear Schrödinger (R-EDNLS) equation. In section 3, the numerical scheme is specified and the results of numerical integrations of equation (3) are presented in section 4. The numerical techniques related to the integration of equation (3) are discussed in detail, as clearing up their mathematical aspects may be helpful in solving numerically NLS equations of a more general type than equation (3). Through the numerical solutions, a precise threshold for collapse is identified in the case of the so-called extended derivative nonlinear Schrödinger (EDNLS) equation, for which γ is zero.

2. Elements of theory

The R-EDNLS equation is given as

$$\partial_t u + \mathrm{i}\partial_x^2 u + |u|^2\partial_x u + \mathrm{i}\gamma u\partial_x|u|^2 + \mathrm{i}\sigma|u|^4 u = 0 \tag{6}$$

where $u(x,t) : \mathbb{R}\times\mathbb{R}_+ \to \mathbb{C}$, while $\gamma \in \mathbb{R}$ and $\sigma \in \mathbb{R}$ denote constants.

The mathematical properties of the R-EDNLS equation are well known in certain special cases. For $\gamma = \sigma = 0$, equation (6) is completely integrable through the inverse scattering transform [6]. For $\gamma = 0$ and $\sigma \neq 0$, equation (6) forms a Hamiltonian system, processing three conservation laws [5]. However, this Hamiltonian structure is lost in the general case $\gamma \neq 0$ and $\sigma \neq 0$, although the mass integral remains conserved [4].

2.1. Conservation laws and the virial identity

In the special case with $\gamma = 0$, the EDNLS equation possesses three conservation laws:

$$\partial_t U_i + \partial_x P_i = 0 \qquad i = 1, 2, 3 \tag{7}$$

where the densities, U_i, and their associated fluxes, P_i, take the form

$$U_1 = |u|^2 \tag{8}$$

$$P_1 = \mathrm{i}(u^*\partial_x u - u\partial_x u^*) + \tfrac{1}{2}|u|^4$$

$$U_2 = \tfrac{1}{2}\mathrm{i}(u^*\partial_x u - u\partial_x u^*) \tag{9}$$

$$P_2 = \tfrac{1}{2}\mathrm{i}(u\partial_t u^* - u^*\partial_t u) + \tfrac{1}{2}|u|^4$$

$$U_3 = |\partial_x u|^2 - \tfrac{1}{4}\mathrm{i}|u|^2(u\partial_x u^* - u^*\partial_x u) - \frac{\sigma}{3}|u|^6 \tag{10}$$

$$P_3 = -(\partial_t u\partial_x u^* + \partial_t u^*\partial_x u) + \mathrm{i}\tfrac{1}{4}|u|^2(u\partial_t u^* - u^*\partial_t u)$$

leading to the conservation of mass, linear momentum, and energy integrals, with the respective densities U_1, U_2, and U_3.

In particular, for $\gamma = 0$, equation (6) forms a Hamiltonian system with the Hamiltonian integral defined as

$$H = \int U_3\,\mathrm{d}x = \|\partial_x u\|_2^2 - \frac{\sigma}{3}\|u\|_6^6 - \tfrac{1}{4}\mathrm{i}\int |u|^2(u\partial_x u^* - u^*\partial_x u)\,\mathrm{d}x. \tag{11}$$

Here, we have introduced the usual notation for Sobolev spaces with the L^p norm:

$$\|f\|_p = \left(\int |f|^p\,\mathrm{d}x\right)^{1/p}$$

and we assume, at least locally in time, that $u \in H^1$.

In the presence of the Raman effect, i.e. for $\gamma \neq 0$, only the mass integral $\int U_1 \, \mathrm{d}x$ remains conserved, while the evolution of the linear momentum, U_2, is described by

$$\partial_t U_2 + \partial_x P_2 = \tfrac{1}{2}\gamma \partial_x^2 |u|^4 - \gamma(\partial_x |u|^2)^2.$$

Let us define the total mass, N, of the wavefield as follows:

$$N = \int |u|^2 \, \mathrm{d}x \tag{12}$$

through which we also define the centre of mass as

$$\langle x \rangle = \frac{1}{N} \int x |u|^2 \, \mathrm{d}x \tag{13}$$

and, likewise, the mean-square width of the wavefield as

$$\langle (x - \langle x \rangle)^2 \rangle = \frac{1}{N} \int (x - \langle x \rangle)^2 |u|^2 \, \mathrm{d}x. \tag{14}$$

Using the conservation laws, equations (11)–(14) and the assumption that the wavefield is localized in space, we arrive at the equations of motion for the centre of mass:

$$N \partial_t \langle x \rangle = 2 \int U_2 \, \mathrm{d}x + \tfrac{1}{2} \int U_1^2 \, \mathrm{d}x \tag{15}$$

and

$$N \partial_t^2 \langle x \rangle = -2\gamma \int (\partial_x U_1)^2 \mathrm{d}x - 2 \int U_1 \partial_x U_2 \, \mathrm{d}x. \tag{16}$$

Moreover, we can derive the equation of motion for the mean-square width of the wavefield:

$$N \partial_t \langle (x - \langle x \rangle)^2 \rangle = \int (x - \langle x \rangle)(U_1^2 + 4U_2) \mathrm{d}x \tag{17}$$

and, finally, the virial identity

$$N \partial_t^2 \langle (x - \langle x \rangle)^2 \rangle = 8H + \tfrac{2}{3}\|u\|_6^6 - 4 \int (x - \langle x \rangle) U_1 \partial_x U_2 \, \mathrm{d}x$$
$$-4\gamma \int (x - \langle x \rangle)(\partial_x U_1)^2 \mathrm{d}x - 2N(\partial_t \langle x \rangle)^2. \tag{18}$$

As will be seen shortly, equations (15)–(18) play an important role in the evaluation of the numerical scheme as well as provide a framework for the discussion of the numerical results.

2.2. Localized solutions

Particular localized solutions to the EDNLS equation, i.e. $\gamma = 0$, may take the form of stationary solutions or steadily propagating travelling wave solutions. The existence of the latter follows from the possibility of a balance between the nonlinearity and the dispersive effect. For time-dependent solutions it should be noted that the nonlinear derivative term introduces a drift of the wavefield, as explained in the preceding section.

In this work we will, for simplicity, focus attention towards the dynamics of wavefields that initially are localized. Indeed, as initial conditions for our numerical studies we use wavefields that are closely related to steady-state solutions of the EDNLS equation. For this, we find it useful to briefly review what is known about such stationary solutions for the R-EDNLS equation in general.

We shall seek stationary solutions to the R-EDNLS equation in the form

$$u(x,t) = \phi(x)\exp(-\mathrm{i}\lambda t). \tag{19}$$

Inserting this into equation (6) yields an ordinary differential equation (ODE) for ϕ as

$$-\mathrm{i}\lambda\phi + \mathrm{i}\phi'' + |\phi|^2\phi' + \mathrm{i}\sigma|\phi|^4\phi + \mathrm{i}\gamma\phi(|\phi|^2)' = 0. \tag{20}$$

In the following we have chosen to split the analysis into the two cases related to the EDNLS and R-EDNLS equations, separately, as their respective results differ from each other.

2.2.1. The case $\gamma = 0$. Let us first consider the case when $\gamma = 0$. As shown by contradiction in [4], only in the case of $\lambda > 0$ can localized smooth solutions exist. We then search for such a particular solution in the form of equation (19) with the complex amplitude, ϕ, assumed to be expressed as

$$\phi(x) = a(x)\exp(\mathrm{i}\theta(x)). \tag{21}$$

Inserting equations (19) and (21) into equation (20) yields a condition on $\theta(x)$, namely

$$\theta' = \tfrac{1}{4}a^2 + \frac{c_1}{a^2} \tag{22}$$

where c_1 is a constant and $a(x)$ must satisfy

$$\tfrac{1}{2}(a')^2 + \Phi(a) = c_2$$

with the potential, $\Phi(a)$, being

$$\Phi(a) = \frac{1}{6}\left(\sigma + \frac{3}{16}\right)a^6 - \frac{1}{4}(2\lambda - c_1)a^2 + \frac{c_1^2}{2a^2}.$$

Let us now seek a localized solution for $c_1 = c_2 = 0$ and $\sigma > -\frac{3}{16}$. The potential then reduces sufficiently to allow us to find a soliton-like solution (henceforth referred to as 'soliton'), with amplitude and phase being given by

$$\begin{aligned}(a(x))^2 &= \sqrt{\frac{48\lambda}{16\sigma+3}}\,\frac{1}{\cosh(2\sqrt{\lambda}(x-x_0))}\\ \theta(x) &= \sqrt{\frac{3}{16\sigma+3}}\,\tan^{-1}(\exp(2\sqrt{\lambda}(x-x_0))).\end{aligned} \tag{23}$$

Inserting this solution into equations (11), (16) and (18) confirms that the solution is stationary with a Hamiltonian $H = 0$.

2.2.2. The case $\gamma \neq 0$. Let us now consider the R-EDNLS equation. We will again seek solutions in the form determined by equations (19) and (21). Introducing this into equation (20) yields an equation for the amplitude a:

$$-\lambda a + a'' - a(\theta')^2 + a^3\theta' + \sigma a^5 + \gamma a(a^2)' = 0 \tag{24}$$

with equation (22) as a condition on the phase θ. Since we are looking for localized solutions we safely assume $c_1 = 0$. After inserting equation (22) into equation (24), the amplitude, a, is found to satisfy the relation

$$-\lambda a + a'' + \left(\sigma + \tfrac{3}{16}\right)a^5 + \gamma a(a^2)' = 0.$$

After multiplying this equation with a' and integrating over $\mathbb{R}$, while assuming that the integration constant is zero as we look for localized solutions, the following condition results

$$\frac{\gamma}{2}\int [(a^2)']^2 \,\mathrm{d}x = 0.$$

Clearly, this condition can only be fulfilled when a is a constant, which contradicts the assumption of localization of non-trivial stationary waves. Consequently, localized smooth wavefields cannot exist as stationary solutions to the R-EDNLS equation. Hence, the effect of the Raman term is to prevent the existence of localized solutions, as they may arise in the EDNLS equation.

Let us finally note that in the general framework of equation (20), from which solutions ϕ are sought with $\lambda > 0$, this eigenvalue λ can be fixed to unity without any loss of generality. This property simply follows from the dilation (scale) transformation $\phi(x) \to \lambda^{1/4}\phi(\lambda^{1/2}x)$, removing λ from equation (20) even when γ differs from zero.

3. Numerical scheme

In order to accurately resolve the dynamics of the R-EDNLS equation we have developed a stable pseudospectral multi-domain method. Spectral collocation methods have been applied extensively in the past for solving nonlinear partial differential equations, often yielding results superior to those obtained by other methods. However, the position of the grid points in the computational grid is predetermined, in particular with clustering close to the boundaries. This clustering of the grid points is known to cause problems for resolving functions with layers interior to the domain. To circumvent this weakness we have chosen to apply a multi-domain method, thereby greatly increasing the flexibility of the grid distribution such that high resolution can be maintained in areas of great variation. As we will learn later, this approach also reduces the computational workload significantly.

The scheme used in each individual domain is based on Chebyshev collocation methods, which, due to their superior approximation properties, are widely used for solving nonlinear partial differential equations.

The Chebyshev polynomial of order k is defined as

$$T_k(x) = \cos(k\cos^{-1}x)$$

where $|x| \leqslant 1$. In the following we will consider collocation methods, where the $M+1$ collocation points are chosen to be the Chebyshev–Gauss–Lobatto points found as the roots of the polynomial $(1-x^2)T'_M(x)$, i.e.

$$x_i = -\cos\left(\frac{i\pi}{M}\right) \qquad 0 \leqslant i \leqslant M.$$

When applying a Chebyshev collocation method, the function, $f(x)$, is approximated by a grid function, $f_i = f(x_i)$, where the grid-points are the Gauss–Lobatto points. We construct a global Mth order Chebyshev interpolant, I_M, to obtain the approximation of the function

$$I_M f(x) = \sum_{i=0}^{M} f_i g_i(x) = \sum_{i=0}^{M} f_i \frac{(1-x^2)T'_M(x)(-1)^{M+i+1}}{c_i M^2(x-x_i)}.$$

To seek approximate solutions, $I_M f(x)$, to a partial differential equation, we need to obtain values of the spatial derivatives at the collocation points. This is accomplished

by approximating the continuous differential operator by a differentiation matrix with the entries

$$D_{ij} = g_j'(x_i)$$

such that the derivative of f at a collocation point, x_i, is approximated by

$$\frac{\mathrm{d}f}{\mathrm{d}x}(x_i) \approx \frac{\mathrm{d}(I_M f)}{\mathrm{d}x}(x_i) = \sum_{j=0}^{M} D_{ij} f(x_j)$$

and likewise for higher derivatives. For the explicit expressions of the entries of the matrix operator and further details on collocation methods, we refer to [7].

Let us now consider equation (6) and introduce the state vector, $\boldsymbol{u} = (u_r, u_i)$, with the usual variable being related as $u = u_r + \mathrm{i}u_i$. With this notation, the R-EDNLS equation transforms into two real coupled partial differential equations (PDEs) as

$$\partial_t \boldsymbol{u} - \mathbf{A}\partial_x^2 \boldsymbol{u} + |\boldsymbol{u}|^2 \mathbf{I}\partial_x \boldsymbol{u} - \sigma |\boldsymbol{u}|^4 \mathbf{A}\boldsymbol{u} - \gamma \partial_x (|\boldsymbol{u}|^2)\mathbf{A}\boldsymbol{u} = 0 \tag{25}$$

where the two matrices are given by

$$\mathbf{A} = \begin{bmatrix} 0 & 1 \\ -1 & 0 \end{bmatrix} \qquad \mathbf{I} = \begin{bmatrix} 1 & 0 \\ 0 & 1 \end{bmatrix}.$$

We note in particular that $\mathbf{A}$ is skew-symmetric, i.e. $\boldsymbol{u}^T \mathbf{A}\boldsymbol{u} = 0$, reflecting the dispersive nature of the equation.

Two problems need to be addressed in order to establish the scheme. As we wish to compute the solution in a finite section of $\mathbb{R}$ we need to obtain open boundary conditions and, once these are obtained, develop a way of imposing them. Secondly, we need to discuss a scheme for the patching of the independent domains to arrive at the final global solution. As we will learn shortly, these problems are all closely related.

3.1. Well posed open boundary conditions

Let us first focus our attention on the development of open boundary conditions. As we are dealing with a high-order method, we require that the boundary conditions with the equations and the data form a well posed problem.

For this purpose, we consider the interval $x \in [-1, 1]$, multiply equation (25) with $\boldsymbol{u}^T$ and integrate over the interval to obtain the condition for well posedness in an 'energy' sense as

$$\tfrac{1}{2}\frac{\mathrm{d}}{\mathrm{d}t}\|\boldsymbol{u}\|_2^2 = [-\tfrac{1}{2}|\boldsymbol{u}|^2 \boldsymbol{u}^T \mathbf{I}\boldsymbol{u} + \boldsymbol{u}^T \mathbf{A}\partial_x \boldsymbol{u}]_{-1}^1 \leqslant 0$$

where we have applied the skew-symmetry of $\mathbf{A}$. If we rewrite this condition as follows:

$$\frac{-1}{2|\boldsymbol{u}|^2}[(|\boldsymbol{u}|^2\boldsymbol{u} - \mathbf{A}\partial_x \boldsymbol{u})^T (|\boldsymbol{u}|^2\boldsymbol{u} - \mathbf{A}\partial_x \boldsymbol{u}) - (\mathbf{A}\partial_x \boldsymbol{u})^T (\mathbf{A}\partial_x \boldsymbol{u})]_{-1}^1 \leqslant 0$$

we immediately obtain the well posed homogeneous boundary conditions as

$$\begin{aligned} &x = -1 : |\boldsymbol{u}|^2\boldsymbol{u} - \mathbf{A}\partial_x \boldsymbol{u} = 0 \\ &x = 1 : \mathbf{A}\partial_x \boldsymbol{u} = 0. \end{aligned} \tag{26}$$

Those represent the type of boundary conditions that are required at the open boundaries, be they subdomain boundaries or physical boundaries.

3.2. A stable penalty method

Solving equation (25) using a Chebyshev collocation method involves seeking an Mth degree polynomial, $\boldsymbol{u}_M = I_M \boldsymbol{u}$, satisfying

$$\partial_t \boldsymbol{u}_M - \mathbf{A}\partial_x^2 \boldsymbol{u}_M + |\boldsymbol{u}_M|^2 \mathbf{I}\partial_x \boldsymbol{u}_M - \sigma |\boldsymbol{u}_M|^4 \mathbf{A}\boldsymbol{u}_M - \gamma \partial_x (|\boldsymbol{u}_M|^2)\mathbf{A}\boldsymbol{u}_M = 0 \tag{27}$$

at the internal collocation points, $x = x_i, i \in [1, \ldots, M-1]$, exactly. The boundary conditions, equation (26), are given by

$$\begin{aligned} &|\boldsymbol{u}_M(x_0)|^2 \boldsymbol{u}_M(x_0) - \mathbf{A}\partial_x \boldsymbol{u}_M|_{x_0} = g_0(t) \\ &\mathbf{A}\partial_x \boldsymbol{u}_M|_{x_M} = g_M(t) \end{aligned} \tag{28}$$

where g_0 and g_M signifies the prescribed boundary condition.

The traditional method of imposing the boundary conditions is to solve equation (27) in the interior of the domain and then enforce the boundary conditions strongly at the boundary points. However, this approach does not take into account the fact that the equation must be obeyed arbitrarily close to the boundary. Furthermore, it has been proven difficult to enforce general Robin boundary conditions consistently when using pseudospectral approximations of nonlinear problems. To overcome these problems, we follow the line of thought initiated in [8, 9] and propose a penalty method for approximating the R-EDNLS equation at the collocation points, $x = x_i, i \in [0, \ldots, M]$, as follows

$$\begin{aligned} \partial_t \boldsymbol{u}_M - \mathbf{A}\partial_x^2 \boldsymbol{u}_M + |\boldsymbol{u}_M|^2 \mathbf{I}\partial_x \boldsymbol{u}_M - \sigma |\boldsymbol{u}_M|^4 \mathbf{A}\boldsymbol{u}_M - \gamma \partial_x (|\boldsymbol{u}_M|^2)\mathbf{A}\boldsymbol{u}_M \\ = -\tau_0 Q_0(x)[|\boldsymbol{u}_M(x_0)|^2 \boldsymbol{u}_M(x_0) - \mathbf{A}\partial_x \boldsymbol{u}_M|_{x_0} - g_0(t)] \\ - \tau_M Q_M(x)[\mathbf{A}\partial_x \boldsymbol{u}_M|_{x_M} - g_M(t)] \end{aligned} \tag{29}$$

where

$$Q_0(x) = \frac{(1-x)T_M'(x)}{2T_M'(-1)} \qquad Q_M(x) = \frac{(1+x)T_M'(x)}{2T_M'(1)}.$$

These two functions have the property of being zero at all the Chebyshev–Gauss–Lobatto collocation points except at the two end points of the domain.

We note that the penalty method as given by equation (29) combines the boundary conditions and the governing equation into one equation. When using such an approach, the boundary conditions are not exactly obeyed at the boundary. However, the method remains spectrally accurate as we will soon illustrate. One may also observe that the scheme is equivalent to the traditional way of imposing boundary conditions as τ_0 and τ_M approach infinity.

The parameters, τ_0 and τ_M, are then determined such that the semi-discrete approximation to the initial-boundary-value problem is asymptotically stable.

To prove stability of the overall scheme we consider the linearized and localized approximation to equation (29). Applying the approach developed in [9] and the skew-symmetry of $\mathbf{A}$, it is straightforward to prove asymptotic stability for the scheme provided

$$\tau_0 = \tau_M = \frac{M^2}{2}.$$

With this we have completed the specification of the scheme in a single domain with open boundary conditions. However, extending this to a multi-domain framework involves nothing more than the realization that the subdomain boundaries may also be viewed as open boundaries, albeit of a rather special kind as the boundary condition is computed in the neighbouring domain. Consequently, to patch the domains together we need to pass information in the form of equation (26) between the domains, substitute these for g_0 and g_M in equation (29) and finally modify the solutions at the individual boundaries.

3.3. Time stepping and diagnostics

For temporal integration we use a fourth-order Runge–Kutta scheme with the boundary conditions and the patching being performed at the intermediate time steps. Following completion of each time step, we enforce global continuity. The time step is computed adaptively as

$$\Delta t \leqslant \mathrm{CFL} \times \min_i \left[\frac{|\boldsymbol{u}_M(x_i)|^2}{\Delta_i x} + \frac{1}{(\Delta_i x)^2} \right]^{-1}$$

where $\Delta_i x$ refers to the local grid spacing. In most computations we use a value of $\mathrm{CFL} = 0.75$.

To compute the conserved quantities defined by equations (8)–(12), we need to compute integrals over the domain. For this we use Clenshaw–Curtis quadrature as

$$\int f(x)\,\mathrm{d}x = \sum_{i=0}^{M} f(x_i) w_i$$

where the weights, w_i, are given in [10]. This quadrature rule is exact for f being a polynomial of at most order M. Exact computation of the L^6 norm in the Hamiltonian, equation (11), thus requires that the quadrature rule is applied on $6M$ collocation points. Computation of the conserved quantities therefore involved interpolation of u and its spatial derivative onto $6M$ collocation points. This approach allows us to compute the integrals exactly.

To verify the performance and accuracy of the scheme we use the equations of motion given in equations (15)–(18). At each time step we compute the values of the temporal derivative from the instantaneous fields. At the same time we compute, at each time step, the actual value of the mass centre and the width of the wavefield u, and then use a fourth-order one-sided finite-difference scheme in time to obtain the approximate values of the temporal derivatives. We define a measure of the error as

$$|f| = \frac{|f^E - f^C|}{|f^E|}$$

where f^E refers to the computation of the quantity, f, using equations (15)–(18), while f^C is computed through the finite-difference approximation in time.

Comparing these two different ways of computing the temporal derivatives of the mass centre and the width of the wavefield provides a very good test on the accuracy of the overall scheme. As we are using an adaptive time step we use a finite-difference scheme with arbitrary grid size as discussed in [11].

3.4. Test of the multi-domain scheme

Let us finally present a test of the complete scheme for $\gamma = 0$, i.e. only for the EDNLS equation, and $\sigma = 1.0$. We use the steady-state solution defined by the expressions (23) with $\lambda = 1.0$ and advance the solution until $t = 1.0$. Although the problem is steady state we deal with it as a fully unsteady problem.

We solve this problem in the domain of $x \in [-8, 8]$ and use different resolution, M, and number of subdomains, K. At the outer boundaries we impose the exact solution while the subdomain boundaries are treated as discussed previously in this section.

In figure 1 we show the L^∞ error between the computed and the exact solution at $t = 1.0$ for various choices of M in K equally sized subdomains. It is clear that the scheme

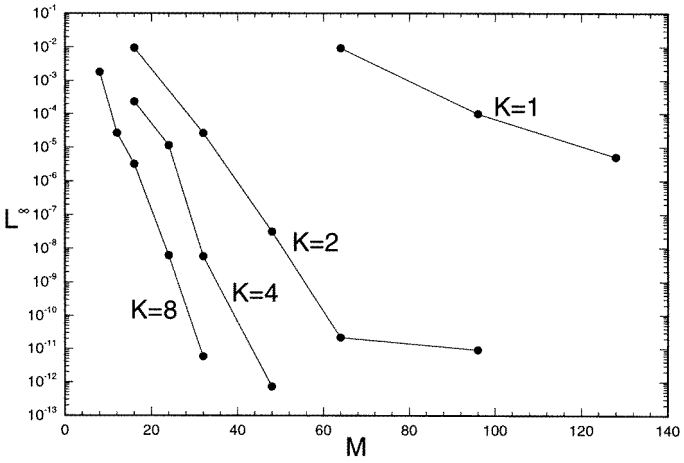

Figure 1. Computation of the L^{∞} error at $t = 1.0$ for various choices of resolution, M, and a number of equally sized subdomains, K.

maintains spectral convergence by M refinements as well as K refinements despite the use of a multi-domain approach. Curiously enough, the one-domain solution, i.e. $K = 1$, requires a very high M to achieve a level of accuracy comparable with that obtained when using several domains. This is caused by the fact that the wavefield is strongly localized in the centre of the domain, a situation that is less fortunate for the one-domain approach. Furthermore, for very high M, effects of round-off errors start to affect the accuracy.

In addition to being more accurate, the multi-domain method is also significantly faster than the one-domain scheme. Performing a 'cost-benefit' analysis as introduced in [12] leads us to the conclusion that $K = 6$ seems to be an optimal choice with respect to computational efficiency, i.e. to the minimization of computing time.

In the remaining part of this paper we will typically consider the interval $x \in [-14, 14]$ and split this into six subdomains as $x_1 \in [-14, -4]$, $x_2 \in [-4, -2]$ and $x_3 \in [-2, 0]$ and symmetrically around $x = 0$. At the open boundaries we simply assume that the wavefield and its spatial derivatives are zero.

4. Numerical results

As initial conditions for our numerical studies we will use a slightly perturbed steady-state solution to EDNLS given in equation (23), such that the structure of the initial wavefield remains unchanged, but the mass, N, may be different from that of the steady-state solution which we name, N_s. The size of the perturbation is measured through the difference between N and N_s.

In all cases we use the parameter $\sigma = 1.0$ in equations (6) and (23). Also, we set $\lambda = 1.0$ without loss of generality, as it proceeds from the scale invariance of equation (20) mentioned at the end of section 2. Computed with the EDNLS soliton amplitude equation (23), the value of N_s is then approximately given by $N_s \simeq 2.5$. Note that N_s remains of the same order of magnitude as the mass associated with the ground state of the CNLS equation, namely $N_0 \simeq 2.72$.

We have chosen to consider the cases of $\gamma = 0$ and $\gamma \neq 0$, separately, as the dynamics is rather different, whether the Raman term is absent or not.

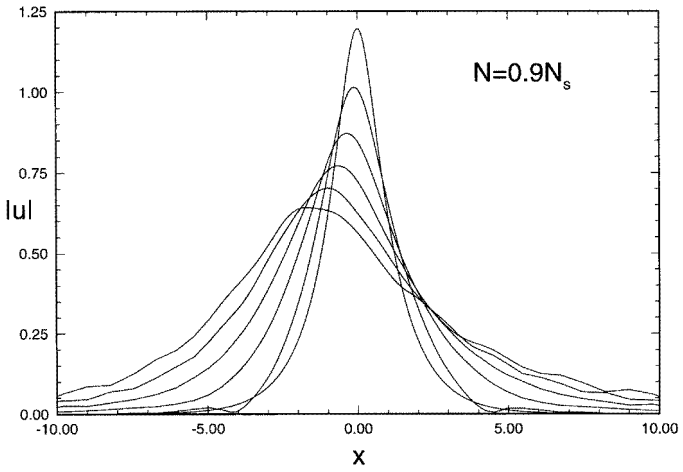

Figure 2. Decaying wavefield with an initial mass of $N = 0.9N_s$. The solution is shown for $t = 0.0$–5.0 with an interval of 1.0.

4.1. The case $\gamma = 0$

The dynamics of the initial wavefield is strongly dependent on the size of the perturbation and we find it illustrative to split the results into three different scenarios.

4.1.1. The subcritical case, $N < N_s$. Let us first consider the case of solutions with a subcritical mass: $N < N_s$. Following [4] we know that the constraint $N < N_c$, where the best attainable estimate of the critical mass is

$$N_c = \frac{3\sigma}{\sqrt{12\sigma^2 + 9\sigma}} N_0 \tag{30}$$

guarantees $H > 0$, such that, governed by equation (18), the solutions may disperse asymptotically in time with an increasing mean width. As introduced in section 1, N_0 denotes the soliton mass for the standard CNLS.

For the actual choice of $\sigma = 1.0$, we obtain $N_c \simeq 0.65N_0 \simeq 0.7N_s$. However, with this estimate, the condition for wave spreading, $N < N_c$, is only a sufficient condition as is indeed illustrated in figure 2 where we show the spreading of the initial wavefield with a mass even slightly exceeding N_c : $N = 0.9N_s$. We have used $M = 24$ in each domain yielding an error as $|\langle x \rangle_t| \sim 10^{-4}$ and $|\langle x \rangle_{tt}| \sim 10^{-2}$, while the mass is conserved to 10^{-6}.

It is clear that, at least for an initial condition with a structure like the soliton solution, the estimate of N_c is conservative. The drift towards negative values of x can be justified from the property explained in section 1, according to which wavepackets move along x with a group velocity possessing a nonlinear contribution ΔV_g^{NL} that evolves like $|u|^2$. In this case, the intensity levels of the localized wavefield decrease, and so does the group velocity of the wavepacket, which forces the latter to move leftward. This behaviour can also be predicted from equation (15).

4.1.2. The critical case, $N \simeq N_s$. Let us now consider the case where $N \simeq N_s$. In fact, we will consider the marginal cases of $N = (1 \pm 0.01)N_s$. The results of long-time integration with $M = 20$ in each domain is shown in figure 3.

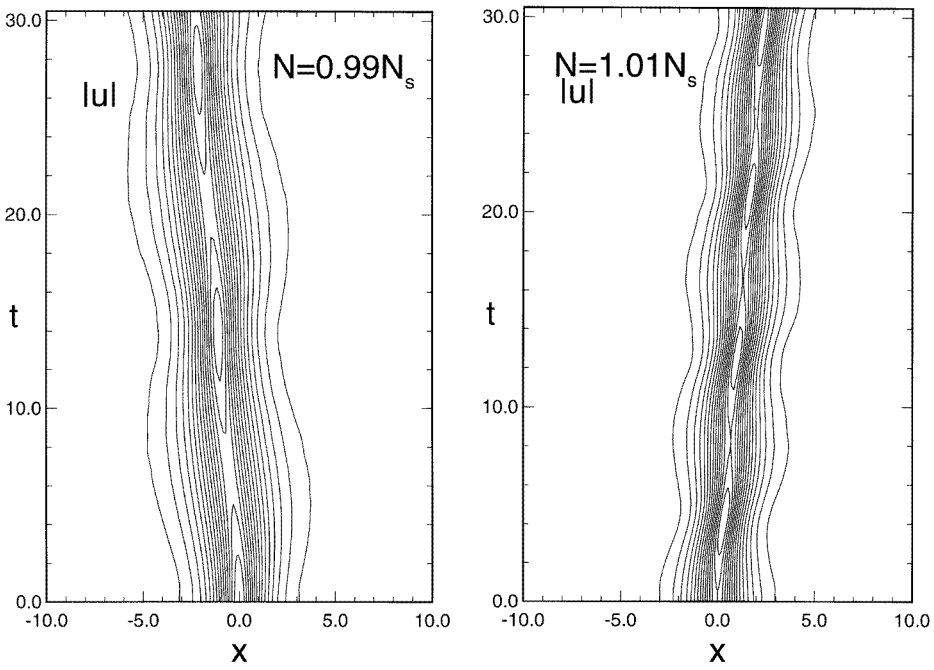

Figure 3. Contour plot of $|u|$ illustrating the temporal development of initially localized wavefields with a mass close to the EDNLS soliton mass, N_s, i.e. slightly less than and more than the soliton mass.

We find that an oscillatory mode appears, drifting leftward and rightward for $N = 0.99N_s$ and $N = 1.01N_s$, respectively. In both situations mass conservation is ensured to 10^{-6}, while the linear momentum and the Hamiltonian are conserved to 10^{-5}. We also find that $|\langle x\rangle_t| \sim 10^{-5}$ and $|\langle x\rangle_{tt}| \sim 10^{-2}$. Again the direction of the drift is as expected from equations (5) and (15). In this situation, it can be explained by means of the perturbed solution $u = (1+\tilde{\epsilon})\phi$, where ϕ denotes the soliton solution defined by equation (23) and $\tilde{\epsilon}$ is a small parameter satisfying $|\tilde{\epsilon}| \ll 1$. By inserting this perturbed solution into equation (15) for the wave centre of mass, it is found that the latter evolves as $N\partial_t\langle x\rangle = \tilde{\epsilon}\|\phi\|_4^4 + o(\tilde{\epsilon}^2)$, after using $\partial_t\langle x\rangle = 0$ on the soliton solution. The previous relations clearly show that $\langle x\rangle$ moves leftward for $\tilde{\epsilon} < 0$ and rightward in the opposite case $\tilde{\epsilon} > 0$.

The oscillatory mode cannot be quantified for the moment, but we may nevertheless view it as a marginal boundary behaviour lying between the asymptotic spreading revealed in section 4.1.1 and the singular collapsing evolution detected below. The exact boundary $N = N_s$ would then correspond to the standing wave soliton solution remaining centred at $x = 0$ for every time and, herein, undergoing no spatial drift.

4.1.3. The supercritical case, $N > N_s$. In [4] it was argued on the similarity between EDNLS and CNLS equations, that one should expect the wavefield to collapse for $N > N_c$, as inferred from the condition $H < 0$, provided the latter requirement be sufficient for assuring the vanishing of the virial integral $\langle(x - \langle x\rangle)^2\rangle$ at a finite time.

In figure 4 we show that this is indeed true at least from the slight perturbation of $N = 1.1N_s > N_c$. The computation is performed with $M = 48$ and, until shortly before the collapse, the mass is conserved to 10^{-9}, while the linear momentum and the Hamiltonian

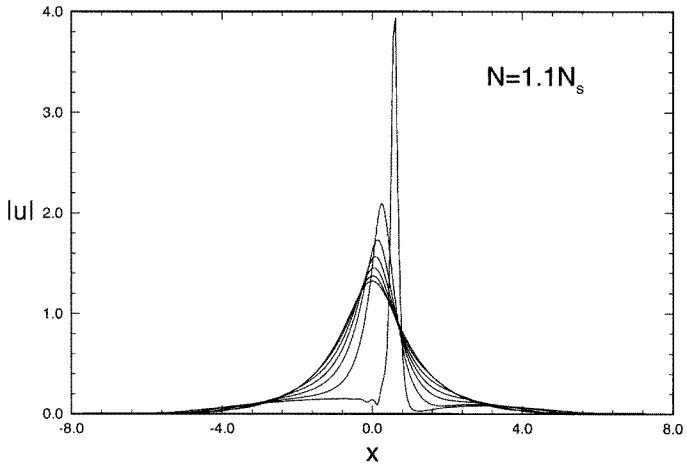

Figure 4. Collapsing solution with an initial mass $N = 1.1N_s$. The magnitude, $|u|$, is shown for time range $t = 0.0$–1.2 with intervals of 0.1.

are conserved to 10^{-6}. We also find that $|\langle x\rangle_t| \sim 10^{-7}$ and $|\langle x\rangle_{tt}| \sim 10^{-5}$. From this figure, we still observe the drift of the wavefield towards positive x, which results from the nonlinear dispersion that participates in the wave group velocity with a positive intensity-dependent contribution. The higher the wave intensity becomes, the more rightward-shifted the wave amplitude is. Besides, compared with the estimate found in [4], the criterion for collapse $N > N_c$ resulting from $H < 0$ has to be exceeded to a small extent, because the nonlinear dispersive contribution may counteract the negativity of the right-hand side of equation (18) which is required to promote the collapse. As anticipated in [4], collapse *may* occur for $N > N_c$ with $H < 0$, but this condition alone seems not sufficient for ensuring the blow-up. Here, the previous numerical simulations allow us to determine accurately the mass threshold for collapse: apart from the tiny perturbations observed in figure 3, this threshold appears to be nothing else but the mass integral computed on the EDNLS soliton solution, N_s, instead of N_c, with $N_s > N_c$.

4.2. The case $\gamma \neq 0$

Let us now consider the more general problem of the dynamics of R-EDNLS solutions. As we have previously discussed, no localized solutions exist for $\gamma \neq 0$.

In the following, we will discuss the dynamics of initially localized wavefields, defined in this case by the steady-state solution to the EDNLS equation, for various values of γ and, in particular, investigate the effect of $\gamma \neq 0$ on the collapse dynamics.

As for EDNLS we have chosen to split the discussion into the three situations of subcritical, critical and supercritical mass, N, as related to the EDNLS ground-state solution with mass N_s.

4.2.1. The subcritical case, $N < N_s$. For the case of a subcritical mass, there are only minor differences between the dynamics of solutions respectively governed by the EDNLS and R-ENDLS equations. In both cases, the solutions disperse rapidly with a spreading of the localized wavefield.

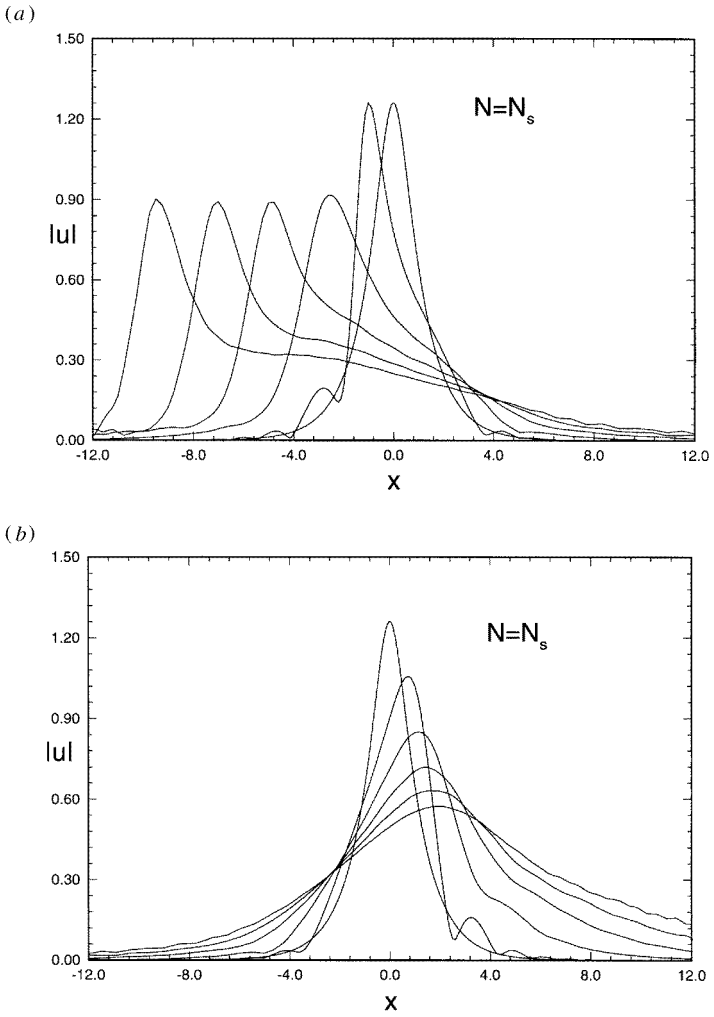

Figure 5. Decaying of the EDNLS soliton for (*a*) $\gamma = 1$ and (*b*) $\gamma = -1$, respectively. The solutions are shown for $t = 0.0$–2.5 with an interval of 0.5.

4.2.2. The critical case, $N = N_s$. The critical case for $N = N_s$ is more interesting. We recall that for $\gamma = 0$ an oscillatory mode appeared for N being slightly perturbed from N_s.

In figure 5 we illustrate the general dynamics observed for $\gamma = \pm 1$ and $N = N_s$. The computations are performed with $M = 24$ in each subdomain and in both cases we assure mass conservation to 10^{-6}, while $|\langle x \rangle_t| \sim 10^{-4}$ and $|\langle x \rangle_{tt}| \sim 10^{-2}$.

The dynamics of the two cases for $\gamma > 0$ and $\gamma < 0$ are rather different, although the final result appears to be the same, i.e. with a spreading and decay of the initially localized wavefield. However, while for $\gamma < 0$ we observe an initial steepening of the wavefield, followed by a uniformly decaying, slightly rightwarded, drifting motion, the situation for $\gamma > 0$ is different. In this case, the initial steepening is followed by a faster leftward drift and a structured solution forms and decays very slowly. Compared with the former solutions to the EDNLS equation, the centre of mass of the wavefields undergoing the Raman effect appears to be strongly shifted to the left for $\gamma > 0$ and more moderately to the right for

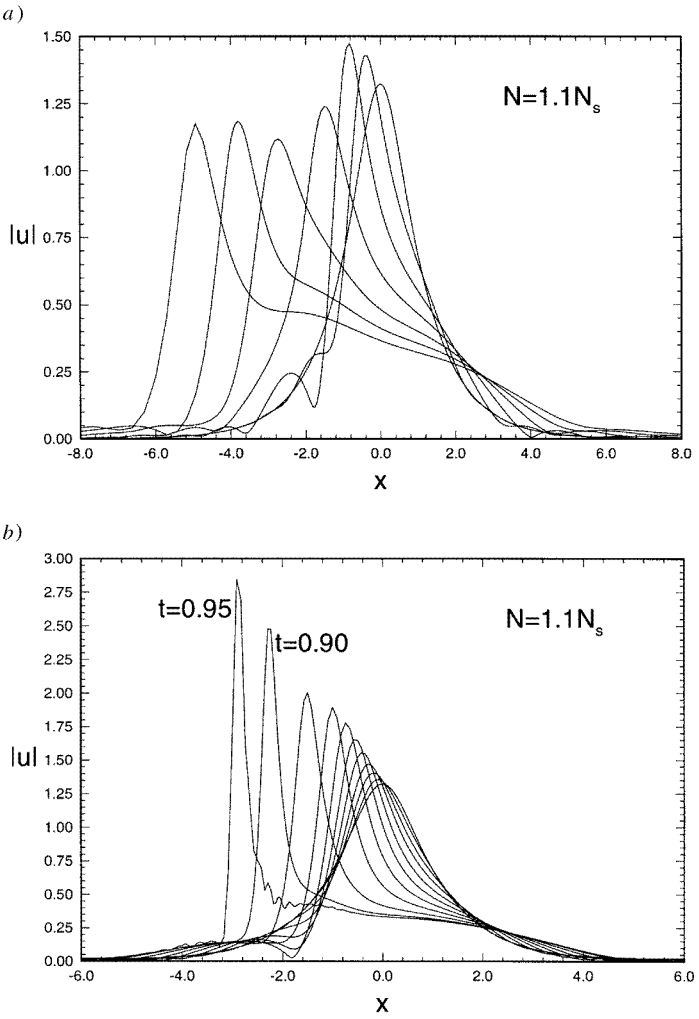

Figure 6. (*a*) The decaying and spreading wavefield for $\gamma = 1$. The solution is shown for $t = 0.0$–1.2 with an interval of 0.2. (*b*) The collapsing wavefield for $\gamma = 0.5$ for $t = 0.0$–0.95 with intervals of 0.1 with the exception of the explicitly marked solutions.

$\gamma < 0$, which is in accordance with the displacement of the wave centroid governed by equation (16). Following the sign of γ, the Raman effect can thus interplay with the natural drift induced by the nonlinear dispersion of the waves.

4.2.3. The supercritical case, $N > N_s$. For $\gamma = 0$ we observed that the wavefield collapses for $N = 1.1N_s$. The situation for $\gamma \neq 0$ is very different, as there is also a significant difference between the cases $\gamma > 0$ and $\gamma < 0$.

Let us first consider the case $\gamma > 0$ and $N = 1.1N_s$. In figure 6 we show the development of the initially localized wavefield for $\gamma = 1.0$ and $\gamma = 0.5$. The computations are done for $M = 36$ yielding a mass conservation to 10^{-8}, while $|\langle x \rangle_t| \sim 10^{-5}$ and $|\langle x \rangle_{tt}| \sim 10^{-3}$.

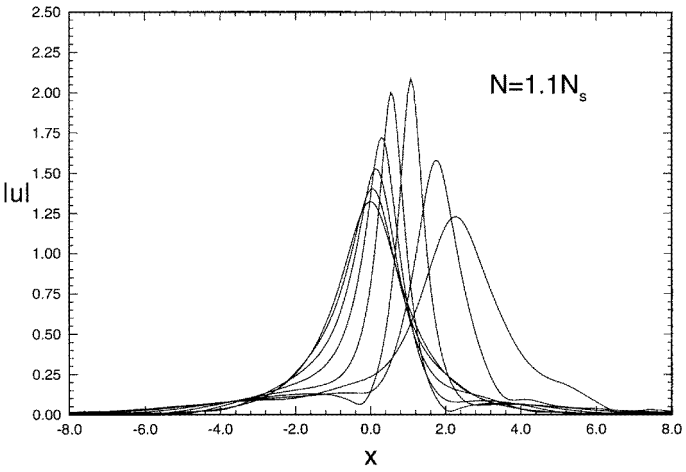

Figure 7. The decaying wavefield for $\gamma = -0.5$ shown for $t = 0.0$–2.1 with an interval of 0.3.

Whereas the wavefield in the case of $\gamma = 1.0$ behaves similarly to that with $N = N_s$, we now observe with $\gamma = 0.5$ that the solution, instead, collapses. Hence, for $\gamma > 0$ it seems that only for γ above a threshold value γ_c can the Raman term inhibit collapse of the initially supercritical wavefield.

The situation for $\gamma < 0$ appears to be completely different. In figure 7 we show the development of the wavefield for $\gamma = -0.5$, i.e. the numerically opposite value to $\gamma = 0.5$ for which collapse takes place. We observe that, following an initial steepening of the wavefield on the route towards a collapse, the effect of the Raman term becomes sufficiently strong to inhibit the collapse. In this case, we have been unable to establish a threshold under which collapse survives the effect of the Raman term. For values as low as $\gamma = -0.01$ the picture qualitatively remains the same, i.e. following an initial steepening, the wavefield finally decays and spreads out. These computations are performed with $M = 40$, yielding a mass conservation to 10^{-8}, while $|\langle x \rangle_t| \sim 10^{-7}$ and $|\langle x \rangle_{tt}| \sim 10^{-3}$. These results confirm the absence of collapse predicted by the Lagrangian approach of equation (3) in [4], for negative values of γ.

5. Concluding remarks

In this work, we have examined the dynamical behaviour of localized solutions to the R-EDNLS equation by means of a stable pseudospectral multi-domain numerical method. This equation can be viewed as a generic model for describing the propagation of short wavetrains in dispersive Kerr-type media promoting high-order nonlinear dispersive effects, as they may take place in monomode dielectric guides. In every situation investigated here, the nonlinear dispersion associated with the β-dependent nonlinear derivative term of equation (3) was displayed to introduce a wave drift along the x axis. This drift has been shown to be related to the nonlinear part of the group velocity of the wave depending on the peak intensity. When the self-induced Raman effect is absent ($\gamma = 0$), solutions have been shown to spread out, or to oscillate, or still to collapse at a finite time, whenever their associated mass integral lies below, around or far above the critical threshold N_s, respectively. This threshold N_s corresponds to the L^2 norm of the soliton solution determined by the expressions (23). By comparison with the theoretical estimates obtained in [4], it was expected that the solution

$u(x,t)$ should surely behave regularly, even disperse like spreading CNLS solutions, when N is smaller than the quantity N_c recalled in equation (30), whereas solutions with mass integrals belonging to the opposite domain $N > N_c$ could collapse. These expectations have here been verified numerically. In addition, while the exact mass threshold for collapse remained undetermined in [4], the present analysis enabled us to fix it in close vicinity of the EDNLS soliton mass N_s, which supports the comparison with blowing up CNLS solutions possessing a mass $N > N_0$. Considering next the Raman effect ($\gamma \neq 0$), it was also predicted in [4] that wave collapse may not be promoted, especially for negative values of γ, as long as this Raman effect could be strong enough to counteract wave self-focusing. Again, this property was here revealed numerically. Nevertheless, collapse appears to possibly develop within a finite range of positive values of $\gamma : 0 \leqslant \gamma \leqslant \gamma_c$. For the initial data investigated in the present work ($N = 1.1N_s$), we found $\frac{1}{2} < \gamma_c < 1$. From this basis, we can anticipate that the threshold γ_c may increase with an increasing N. However, determining accurately this threshold as a function of the initial mass for a given wavefield remains an open problem.

Acknowledgments

JSH gratefully acknowledges the support of NSF grant no ASC-9504002 and DoE grant no DE-FG02-95-ER25239. He would also like to express gratitude for support by the Risø National Laboratory, Optics and Fluid Dynamics Department, during an extended stay at which some of this work was done. This work is supported by the Danish Natural Research Council (SNF).

References

[1] Newell A C and Moloney J V 1991 *Nonlinear Optics* (Redwood City, CA: Addison-Wesley)
[2] Kodama Y and Hasegawa A 1987 *IEEE J. Quantum Electron* **QE-23** 510
[3] Gromov E M and Talanov V I 1996 *Zh. Eksp. Teor. Fiz.* **110** 137 [1996 *Sov. Phys.–JETP* **83** 73]
[4] Bergé L, Juul Rasmussen J and Wyller J 1996 *J. Phys. A: Math. Gen.* **29** 3581
[5] Flå T and Wyller J 1993 *Phys. Scr.* **47** 214
[6] Kaup D J and Newell A C 1978 *J. Math. Phys.* **19** 798
[7] Funaro D 1992 *Polynomial Approximation of Differential Equations* (New York: Springer)
[8] Funaro D and Gottlieb D 1988 *Math. Comp.* **51** 599
[9] Hesthaven J and Gottlieb D 1996 *SIAM J. Sci. Comput.* **17** 579
[10] Canuto C, Hussaini M Y, Quarteroni A and Zang T A 1987 *Spectral Methods in Fluid Dynamics* (New York: Springer)
[11] Fornberg B 1988 *Math. Comp.* **51** 699
[12] Hesthaven J 1997 *SIAM J. Sci. Comput.* **18** 658